53rd AIAA/ASME/ASCE/AHS/ASC Structures, Structural Dynamics and Materials Conference
20th AI
23 - 26 April 2012, Honolulu, Hawaii

AIAA 2012-1358

Level Set Based Topology Optimization with Stress Constraints and Consistent Sensitivity Analysis

Alexander Verbart*

National Aerospace Laboratory (NLR), Amsterdam, The Netherlands

Matthijs Langelaar†, Nico Van Dijk†, Fred van Keulen†

Delft University of Technology, Delft, The Netherlands

For aeronautical applications of topology optimization, it is of importance to develop topology optimization techniques, that can handle stress constraints in an efficient and accurate manner. The development of such topology optimization techniques is a challenging task due to the local nature of the stress constraints, their highly non-linear behaviour with respect to the design variables and the so-called singularity phenomenon. An accurate sensitivity analysis is essential for these type of problems with multiple constraints.

In this paper, we propose a methodology of dealing with stress constraints in a level set based framework. In this framework, the level set function nodal values are related to element densities by an exact Heaviside projection. Stress relaxation and constraint aggregation techniques are used to deal with the singularity phenomenon and the local nature of the stress, respectively. A constrained optimization problem is then solved, in which the design variables (the level set nodal values) are updated in the projected steepest-descent direction, which is determined using a consistent sensitivity analysis.We demonstrate the effectiveness of this technique on two numerical examples. The results show that the level set method with a consistent sensitivity analysis allows for the treatment of multiple constraints by using constrained optimization techniques.

Nomenclature

$(.)_e$	Subscript indicating element defined quantaties
α	Angle of attack
$\boldsymbol{\rho}$	Design variable vector with densities
$\boldsymbol{\sigma}$	Stress vector
$\boldsymbol{\varepsilon}$	Strain vector
Δc	Update step scaling
Γ	Structural boundary
$\mathbf{C}$	Elasticity tensor
$\mathbf{f}$	Load vector
$\mathbf{K}$	Global stiffness matrix
$\mathbf{K}_e$	Element stiffness matrix
$\mathbf{u}$	Nodal displacement vector
Ω	Design domain
Ω_{mat}	Material domain
ϕ	Level set function
σ_{PN}	P-norm approximation of maximum stress
$\rho_{\min}$	Minimum density
$\sigma^{\max}$	Maximum local stress value
$\sigma_{\lim}$	Maximum allowable stress
$\tilde{(.)}$	Superscript indicating a qp-relaxed state of the variable
C	Sum of the compliances
c	Scaling factor
E	Young's modulus
E^*	Effective Young's modulus
g	Constraint
H	Heaviside function
m	Number of group constraints
n	Number of design variables
P	Exponent P-norm approximation
p	Exponent SIMP law
q	Exponent $qp-$approach
V	Volume fraction

*PhD researcher, NLR, AVCE, Anthony Fokkerweg 2, Amsterdam, The Netherlands.
†Delft University of Technology, Mekelweg 2, Delft, The Netherlands.

I. Introduction

The grown demand of lightweight structures in aeronautics, driven by fuel cost savings, emission reduction and improved flight performance, makes design optimization an even more important discipline for the aircraft industry. Since aircraft components typically operate under multiple loading conditions, it is difficult to rely only on engineering intuition to decide where to remove material and simultaneously meet all structural requirements (e.g. stress and buckling criteria). This makes topology optimization a potentially powerful tool to assist the design of aircraft components.

One of the challenges in topology optimization is the inclusion of stress constraints. Traditionally, most work in continuum density-based topology optimization (e.g. SIMP[1,2]), focuses on the minimum compliance design. The reason for this is its well-established problem formulation which can be solved efficiently by mathematical programming techniques.[3] Therefore, real-world applications of topology optimization are usually based on the minimum compliance design, followed by shape optimization to satisfy stress and buckling criteria.[4] It is known that for a limited class of problems, the minimum compliance design is equivalent to the stress-based design.[5] However, real-world applications, often subjected to multiple loading conditions, do typically not belong to this class of problems.

When considering stress constraints additional difficulties have to be addressed, such as the local nature of the stress, whereas compliance is a global measure. This leads to a computationally expensive problem in which the number of constraints might be of the same order as the number of design variables. Furthermore, in density-based topology optimization, problems arise related to the non-uniquely defined stress for intermediate densities and the occurrence of singular optima, which cannot be reached by a typical gradient-based optimizer. The existence of singular optima is known from truss optimization (e.g. in Refs. 6, 7) and is related to the fact that the allowable stress is discontinuous at zero density/area representing void material. This yields a solution containing substantial regions with intermediate densities, whereas a crisp solid/void result is typically desired.

A variety of techniques have been proposed to deal with the difficulties discussed above. For example, constraint aggregation techniques that are based on making a global approximation of the local stress constraints (P-norm,[8] KS-function[9]), thereby drastically reducing the number of constraints and, thus, the costs of sensitivity analysis. To solve the problem of having a non-uniquely defined stress for intermediate densities, Duysinx and Bendsøe proposed an empirical model that mimics the behaviour of porous layered material.[10] Finally, different formulations have been proposed to deal with the singularity phenomenon. In general, these formulations are based on various forms of relaxation of the constraint functions, e.g. relaxation by using smooth envelope functions,[11] ε-relaxation approach[12] and qp-approach.[13]

In this paper, we want to explore the potential of level set based optimization for stress-constrained problems. Depending on the design discretization in level set based optimization, intermediate densities are avoided or limited to a small band along the boundary. We expect this can be an attractive feature for stress-constrained problems. In this paper, we solve the stress-constrained problem following an explicit level set method and consistent sensitivity analysis.[14,15] An exact Heaviside function is used to relate the material fractions/densities to the level set function and we derive the sensitivities with respect to the level set nodal values. The method can be regarded as density-based topology optimization in which the element densities are controlled by the level set function. Techniques introduced to deal with stress constraints in density-based methods (e.g. stress relaxation) will also be used in the current approach.

Only limited work has been done on using a level set method to solve stress-constrained problems.[16,17] The reason for this is that many level set methods solve an unconstrained optimization problem, while adding the constraint(s) to the objective function by a penalty term. In the case of multiple constraints, this can cause difficulties in the optimization process. The novelty of the present approach is that, by using a consistent sensitivity analysis, we formulate the problem as a constrained optimization problem and are able to treat multiple stress constraints.

In this paper, first we introduce the level set method in Section II. Then, we discuss the stress constraint implementation, followed by two numerical benchmark examples which are solved using our level set based optimization algorithm. First, we consider the L-bracket benchmark in Section IV, where we minimize its weight subjected to (multiple) stress constraints. Then, we consider an airfoil shape in Section V, which is subjected to two loading conditions which correspond to two different angles of attack. We perform weight minimization subjected to stress constraints considering the loading conditions, individually and combined. Furthermore, the airfoil is also optimized towards a minimum compliance design subjected to a mass constraint. Finally, inSection IV the conclusions and suggestions for future research are presented.

II. Level set method using a consistent sensitivity analysis

In topology optimization, the aim is to find the optimal material distribution Ω_{mat} inside a larger design domain Ω. When using a level set method to solve this material distribution problem, the material domain and the structural boundary can be described by the level set function $\phi(\mathbf{x})$ as shown in Figure 1.

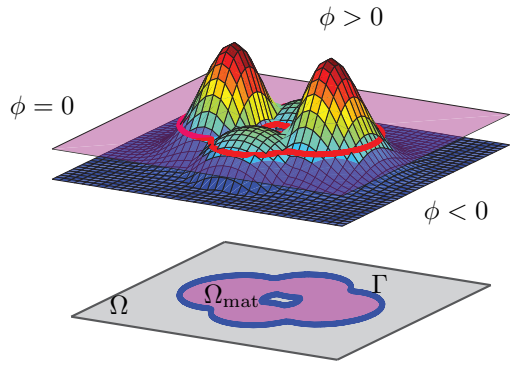

$$\begin{aligned} \phi(\mathbf{x}) &> 0 \quad \forall \mathbf{x} \in \Omega_{\text{mat}} \\ \phi(\mathbf{x}) &< 0 \quad \forall \mathbf{x} \in \Omega \backslash \Omega_{\text{mat}} \\ \phi(\mathbf{x}) &= 0 \quad \forall \mathbf{x} \in \Gamma \end{aligned}$$

Figure 1: On top the level set function $\phi(\mathbf{x})$ cut by the zero level plane. Below the material domain Ω_{mat} and the structural boundary Γ described by the level set function, shown on the design domain Ω.

The structural boundary Γ is described implicitly as the zero isocontour of the level set function ($\phi(\mathbf{x}) = 0$) and the material domain Ω_{mat} is given by $\phi > 0$. A change of the level set function results in a change of shape (and potentially of topology) of the material domain Ω_{mat}. As in most level set based topology optimization methods, a fixed finite element mesh is used for the design discretization and the level set ϕ nodal values (design variables) are mapped to a volume fraction/density ρ_e for each finite element. This density represents the presence of material in each element. In this paper, this relation is defined as,

$$\rho_e(\phi) = \rho_{\min} + (1 - \rho_{\min}) \frac{\int_{D_e} H(\phi) dA}{\int_{D_e} dA}, \tag{1}$$

where $H(\phi)$ is the Heaviside function and D_e is the element domain. In most level set methods this relation is evaluated by introducing an approximate Heaviside function (e.g. Refs. 18,19). However, in this paper we use the level set method proposed by van Dijk et al[14] in which the exact Heaviside function is used. We also refer to this work for a detailed explanation of the calculation of Eq. (1). Once the relationship is established between the element density and the level set nodal values, the material distribution can be changed by changing the level set function. Typically, in level set based optimization methods in which the level set function is mapped to element densities, the Ersatz material approach is used and the material properties for each element are then scaled with the density.[18,20] Here, SIMP is used and the effective Young's Modulus, E^*, is defined as,

$$E_e^* = \rho_e^p E_0, \quad \text{where,} \quad \rho_e \in [\rho_{\min}, 1] \text{ and } p > 0. \tag{2}$$

Here E_0 is the Young's Modulus associated with 'solid material' elements ($\rho = 1$) and $\rho_{\min}$ is a lower bound close to zero to avoid singularity of the global stiffness matrix. Note that $p > 1$ to penalize intermediate densities.[a] It is known that SIMP penalization is introduced to avoid large grey area's of intermediate densities. Although, in this level set method intermediate densities are limited to a small band along the boundary, similar numerical artefacts were observed. The level set function tends to form small islands, thereby increasing the presence of intermediate densities.[14] The linear structural problem is now defined as,

$$\mathbf{K}(\boldsymbol{\rho})\mathbf{u} = \mathbf{f}, \quad \text{where,} \quad \mathbf{K}(\boldsymbol{\rho}) = \sum_{e \in \Omega} \rho_e^p(\phi) \mathbf{K}_e^0, \tag{3}$$

where $\mathbf{K}$ is the global stiffness matrix which, $\mathbf{u}$ the vector with nodal displacements and $\mathbf{f}$ is the applied load vector.

[a] If $p = 1$ the method becomes the same as the Ersatz material approach.

III. Stress constraint implementation: local and global approach

In our stress constraint implementation, we use the *qp*-approach[13] to relax the stress to circumvent problems of singular optima. Furthermore, computational costs are reduced by applying constraint aggregation techniques,[8] in combination with scaling to account for the overestimation of the maximum local stress. Finally, also group constraints are considered to have a better local control over the stress level.[21,22] Next, these techniques are discussed briefly and the general stress-based optimization design problem is formulated.

A. Stress relaxation

One of the difficulties when considering stress constraints is the non-uniquely defined stress for intermediate densities. Depending on the definition of the stress, this may lead to an all void design or problems with singular optima. Different choices have been presented for the stress definition. For an overview of these different stress definitions we refer to Le et al.[21] In this paper, we consider the *qp*-approach[13] for which the relaxed stress vector $\tilde{\boldsymbol{\sigma}}$ is defined as,

$$\tilde{\boldsymbol{\sigma}} = \frac{\boldsymbol{\sigma}}{\rho^q}, \qquad \text{where,} \qquad q \in (0, p). \tag{4}$$

In this formulation, the exponent q is chosen within the interval $(0, p)$, and, consequently zero stress is imposed for zero density. Lower values of q increase the amount of relaxation. Furthermore, $\boldsymbol{\sigma}$ is the stress vector consistent with the effective Young's modulus E^* in Eq. (2). The stress vector is defined as,

$$\boldsymbol{\sigma} = \mathbf{C}(E^*)\boldsymbol{\varepsilon}, \tag{5}$$

where $\mathbf{C}$ is the elasticity tensor and $\boldsymbol{\varepsilon}$ the strain vector. Substituting (5) together with (2) in Eq. (4) gives,

$$\tilde{\boldsymbol{\sigma}} = \rho^{p-q}\boldsymbol{\sigma}_0, \qquad \text{where} \qquad \boldsymbol{\sigma}_0 = \mathbf{C}_0\boldsymbol{\varepsilon}, \qquad \text{and} \qquad q \in (0, p), \tag{6}$$

where $\mathbf{C}_0$ is the elasticity tensor and $\boldsymbol{\sigma}_0$ is the stress vector for solid material. This interpolation scheme prevents the occurrence of singular optima since the stress becomes zero as the density tends to zero.

In the numerical examples in this paper, the Von Mises stress is considered. Following Eq. (4), the relaxed Von Mises stress for each element, is defined as $\tilde{\sigma}_e = \rho_e^{p-q}\sigma_0$, where σ_0 is the Von Mises stress considering solid material properties. The relaxed local stress constraint is then defined as,

$$\tilde{\sigma} = \rho^{p-q}\sigma_0 \leq \sigma_{\text{lim}}, \quad \text{with,} \quad 0 < q < p, \tag{7}$$

where σ_{lim} is the allowable stress. Note that Eq. (7) is always satisfied for any q in the interval $(0, p)$ and a sufficiently small ρ. This solves the problem of the presence of singular optima. However, the design space is highly non-convex and it may be difficult to find an optimal solution.[23] Note, that Eq. (7) generally has to hold for every element. Consequently, the number of constraints becomes of the order of the number of design variables which leads to computationally expensive problem. In this paper, to reduce the sensitivity analysis costs, aggregation functions are used to approximate the maximum local stress.

B. Global approximation of maximum stress

Next, we will discuss constraint aggregation used for reducing the sensitivity analysis costs. The local stress constraints can be replaced by a global constraint using aggregation functions. First, let us define $\tilde{\boldsymbol{\sigma}}_{\text{vm}}$ as the vector in which the local stresses $\tilde{\sigma}_e$ are stored, i.e. $\tilde{\boldsymbol{\sigma}}_{\text{vm}} = [\tilde{\sigma}_e]_{e\in\Omega}$. The basic idea is that the maximum local stress, $\tilde{\sigma}^{\max} = \max(\tilde{\boldsymbol{\sigma}}_{\text{vm}})$, which is non-differentiable, is approximated by a smooth global aggregation function. Here, the P-norm approximation[10] is used for the maximum local stress which is defined as,

$$\sigma_{\text{PN}} = \left(\sum_{e\in\Omega} \tilde{\sigma}_e^{\text{P}}\right)^{1/\text{P}}. \tag{8}$$

As $\text{P} \to \infty$, the P-norm approaches the maximum stress, $\sigma_{\text{PN}} \to \tilde{\sigma}_{\max}$, whereas lower values overestimate the maximum stress value. However, for a large value of P the aggregated function is highly non-linear, which leads to slow convergence or no convergence at all. Therefore, typically a moderate value of P is

chosen to obtain a more smooth approximation. Using the P-norm approximation, the local constraints can be replaced by a single global constraint,

$$\sigma_{\mathrm{PN}} \leq \sigma_{\mathrm{lim}}. \tag{9}$$

Since a moderate value of P is used, the maximum local stress is overestimated and, consequently, this relation will lead to a too conservative design. To correct for the overestimation of the maximum local stress, a solution strategy was proposed by Le et al.[21] in which the P-norm is normalized/scaled adaptively towards the actual maximum local stress. Instead of the condition in Eq. (9), the following condition has to hold,

$$c\sigma_{\mathrm{PN}} \leq \sigma_{\mathrm{lim}}, \tag{10}$$

where c is a scaling factor which is updated during optimization such that the scaled P-norm converges to the actual maximum stress. For the adaptive scaling factor the following update scheme is introduced,

$$c_{\mathrm{k+1}} = c_{\mathrm{k}} - \Delta c, \quad \text{where,} \quad \Delta c = c_{\mathrm{k}} - \left(\frac{\tilde{\sigma}^{\max}}{\sigma_{\mathrm{PN}}} \right)_{\mathrm{k}}, \tag{11}$$

where Δc is the step size which is bounded to avoid excessive oscillations and k indicating values for the current iteration, in this paper we used: $[-0.05, 0.05]$.

C. Group constraints

Finally, to have a better control over the local stress level, one also could use an intermediate approach, in which several aggregated stress functions are considered.[21,22] This can be achieved by dividing the domain Ω in several subdomains Ω_j for $j = 1...m$, where m is the number of groups. These groups do not necessarily have to be physical/geometrical regions. In this paper, this subdivision is based on maximizing the difference in magnitude of the individual stress values within each group.[21] The local stresses are stored over the groups as follows: 1) first the vector with local stresses $\tilde{\boldsymbol{\sigma}}_{\mathrm{vm}}$ is sorted by magnitude, 2) the entries of this sorted stress vector are subdivided over the subdomains as, $\Omega_j = \{\sigma_j, \sigma_{j+m}, \sigma_{j+2m}...\}$ for $j = 1..m$, where j is the index which gives the location in the sorted vector of $\tilde{\boldsymbol{\sigma}}_{\mathrm{vm}}$. Consequently, the P-norm is a more accurate approximation for the maximum local stress within each group.

Finally, the general form of the design problem, including group constraints is then defined as,

$$\begin{aligned} \min_{\boldsymbol{\phi}} V &= \frac{1}{n} \sum_{e=1}^{n} \rho_e \\ g_j &= \frac{c_j \sigma_{\mathrm{PN},j}}{\sigma_{\mathrm{lim}}} - 1 \leq 0, \quad \text{for} \quad j = 1..m \\ & \rho_{\min} \leq \rho_i \leq 1, \qquad \text{for} \quad i = 1..n, \end{aligned} \tag{12}$$

where the objective function V is the volume fraction to be minimized, and n and m are the number of design variables and groups, respectively. When $m = n$ we return to the local stress-constrained problem where the number of constraints equals the number of design variables, and for $m = 1$ we treat a single global constraint function.

Note that both the adaptive scaling and the fact that group constraints change between iterations (since the order of $\tilde{\boldsymbol{\sigma}}_{\mathrm{vm}}$ changes) do introduce inconsistencies in our optimization algorithm. The influence of adaptive scaling on convergence is largely depend on the chosen update scheme. Here, this effect is limited by choosing small bounds on its update in Eq. (11).

IV. Numerical benchmark study: L-bracket

The algorithm was tested on the L-bracket example shown in Figure 2(a). This example has been used extensively to study stress constrained topology optimization due to its tendency to form a peak stress in its reentrant corner. See Ref. 21 for an overview of various L-bracket designs. Here, the design optimization problem formulated in Eq. (12) was solved. First, the case for a single aggregated stress constraint ($m = 1$) was considered. Then, the number of group constraints (i.e. $m > 1$) was varied to show the effectiveness of the level set method for treating multiple constraints and to study the effect of taking more than one group constraint in combination with scaling.

For all examples, plane stress linear elasticity is considered and the design domain is discretized by quadrilaterals with bilinear shape functions. Furthermore, the level set mesh coincides with the finite element mesh. A Young's modulus of $E = 100$ and a Poisson's ratio of $\nu = 0.3$ are used. For the optimization problem the allowable stress is set to: $\sigma_{\text{lim}} = 2$ and for each case we start with the initial design shown in Figure 2(b). The following set of parameters is used for the stress constraint implementation: the exponent of the P-norm is set to P = 12, the penalization exponent of the SIMP law is chosen as $p = 3$ and the relaxation parameter to $\varepsilon_{qp} = p - q = 0.8$. Finally, the constrained optimization problem is solved using a gradient projection method based on a fixed density change in every iteration (0.1).[14] For a fair comparison, every design problem was solved for a fixed number (400) of topology optimization iterations.

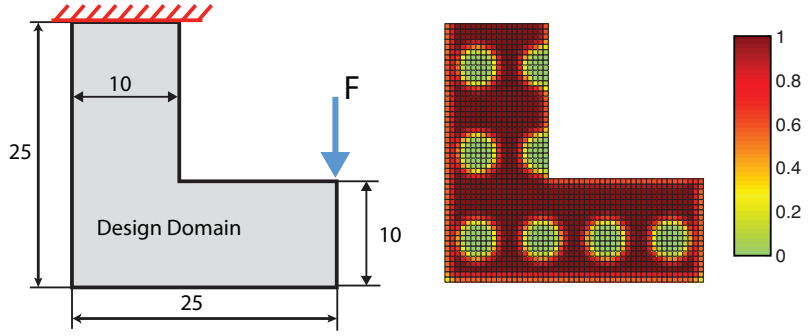

(a) L-bracket. (b) Density distribution.

Figure 2: (a) L-bracket: clamped on the top and forced downwards on the right end. For the design discretization of the design domain a fixed finite element mesh of 1600 quadrilaterals is used (50 elements along the largest sides in both horizontal and vertical direction). (b) the density distribution for the initial design, where red represent solid material elements and green represents the void material elements.

A. Single aggregated stress constraint

First, the L-bracket was optimized for a single aggregated stress constraint. The optimized design and its corresponding Von Mises stress field are shown in Figure 3. An optimized design was obtained of a relative volume of $V = 42.29\%$. Furthermore, the maximum stress is $\tilde{\sigma}^{\max} = 2.00$, and converged to the maximum allowable stress. It can be seen that the optimized design has a rounded shape along the reentrant corner, which effectively prevents the occurrence of peak stresses.

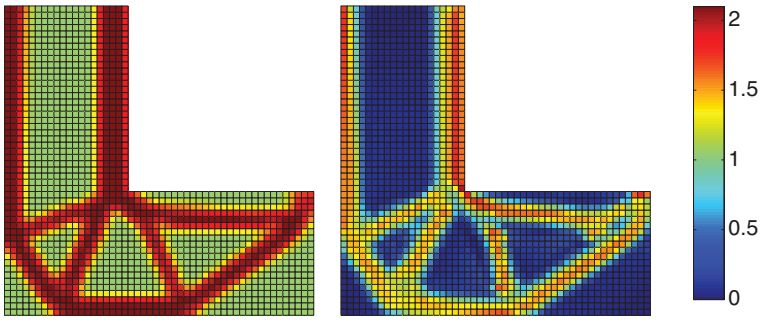

(a) Density distribution. (b) Von Mises stress.

Figure 3: L-bracket: minimizing volume subjected to a single aggregated (P-norm) stress constraint.

B. Group constraints

Next, the L-bracket is optimized using different number of group constraints, as described in Section III. We solve the design problem in Eq. (12) for $m = \{2, 4, 8, 16, 32, 64\}$. The results are listed in Table 1, including the data for a single aggregated constraint. Also the mean stress of each structure is listed, where the mean

stress is used as a measure to compare uniformity of the stress distribution between designs. In Figure 3 the optimized design and corresponding stress field is shown for $m = \{4, 8, 16, 32\}$.

Table 1: Volume minimization subjected to groups stress constraints.

Case				
Objective	Constraints	Volume (%)	$\max \sigma_{\text{vm}}$	mean σ_{vm}
Volume	1 group σ_{PN}	42.29	2.00	0.68
Volume	2 groups σ_{PN}	41.55	2.00	0.70
Volume	4 groups σ_{PN}	40.07	2.00	0.73
Volume	8 groups σ_{PN}	38.74	2.01	0.76
Volume	16 groups σ_{PN}	41.09	2.01	0.77
Volume	32 groups σ_{PN}	41.16	2.01	0.78

From the data listed in Table 1, it can be seen that all design converged to the maximum allowable stress σ_{lim}. Furthermore, it can be seen that, initially increasing the number of group constraints, lead to more optimal designs in terms of volume objective. However, after a certain number of groups the optimized design became less optimal again. This might be related to the constraint handling capabilities of the applied optimizer. The same effect was observed in Ref. 21 where MMA was used as an optimizer. Thus, there seems to exist an optimum number of groups to reach the most optimal design for a given design problem and optimizer. For this problem, the most optimal design was obtained for 8 group constraints. Furthermore, it was observed that the inconsistencies introduced in the optimization algorithm by constraint swapping and scaling also have a negative effect on the convergence. This will be discussed in subsection C.

Note that the mean stress in Table 1, which is used as a measure of the uniformity of the stress distribution, did increase. This increase of the mean stress is difficult to see by comparing the stress field in Figure 3 since the differences are relatively small. However, it is particularly noticeable by comparing the stress distribution for a single constraint and the result for 32 group constraints in Figure 4(h).

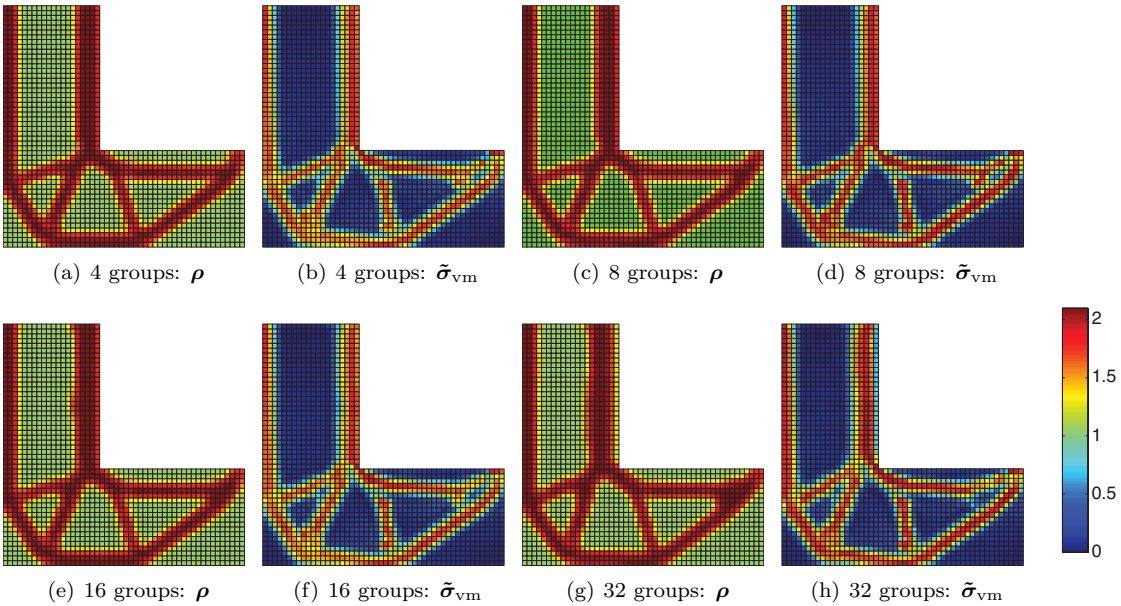

(a) 4 groups: $\boldsymbol{\rho}$ (b) 4 groups: $\tilde{\boldsymbol{\sigma}}_{\text{vm}}$ (c) 8 groups: $\boldsymbol{\rho}$ (d) 8 groups: $\tilde{\boldsymbol{\sigma}}_{\text{vm}}$

(e) 16 groups: $\boldsymbol{\rho}$ (f) 16 groups: $\tilde{\boldsymbol{\sigma}}_{\text{vm}}$ (g) 32 groups: $\boldsymbol{\rho}$ (h) 32 groups: $\tilde{\boldsymbol{\sigma}}_{\text{vm}}$

Figure 4: Material distribution and Von Mises stress field for different numbers of group constraints: (a-b) 2 groups, (c-d) 4 groups, (e-f) 8 groups,(g-h) 16 groups.

C. Convergence history

As discussed in Section III, for the stress constraint implementation the following measures were applied: division into group constraints and scaling. Both measures lead to inconsistencies. The division in group constraints also introduces inconsistencies since its subdivision is based on the order of the magnitudes of the stress values, therefore the composition of these groups changes between iterations. We will refer to this as 'constraint swapping'. In this section, we examined the effect of these inconsistencies on the convergence history. This was done by comparing convergence histories of the L-bracket problem for a single aggregated stress constraint and for the case with 4 group constraints. Both cases are considered without and with scaling. For scaling the update scheme in Eq. (11) was used. The results are shown in Figure 5 where the normalized objective function is plotted and the constraint function versus iteration history. For the sake of clarity, the constraint functions are scaled 100×.

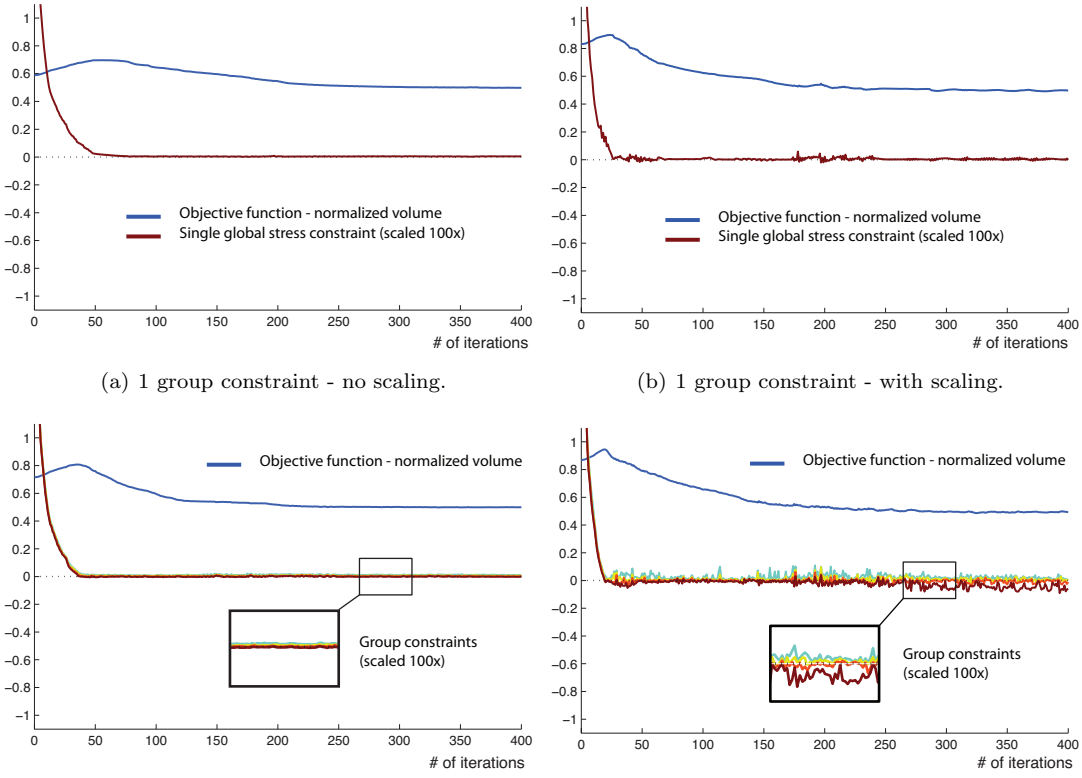

(a) 1 group constraint - no scaling.

(b) 1 group constraint - with scaling.

(c) 4 group constraints - no scaling.

(d) 4 group constraints - with scaling.

Figure 5: Convergence history with and without scaling: (a-b) convergence history for a single group constraint. (c-d) convergence history for four group constraints. Note that the response functions of the constraints are scaled 100 times for the sake of clarity.

It can be seen, by comparing the results for 1 group constraint and 4 group constraints without scaling in Figure 5(a) and Figure 5(c), respectively, that constraint swapping itself has a small or no effect on the smoothness of convergence. However, when comparing both cases again but now *with* scaling in Figure 5(b) and Figure 5(d) it can be seen that the effect of scaling on the smoothness of convergence becomes larger as the number of groups increases.

This negative influence on the convergence, for the combination of swapping and scaling of each group constraint, can be explained by the fact that the composition of each group changes between iterations. Therefore, the scaling factor, determined in the previous iteration to scale the current aggregated stress function is not valid anymore. In theory, close to convergence this effect should vanish since the order of the stress distribution does not change anymore. In practice, it was observed that this effect remains since even a single change in magnitude can lead to a completely different redistribution in groups.

V. Numerical case study: 2D-Airfoil Model

In this section, we consider a symmetrical NACA 0030 airfoil subjected to two loading conditions, shown in Figure 6. The airfoil is supported along the boundaries of the grey region. The aim is to weight-minimize the interior structure. First, volume minimization subjected to a global stress constraint will be performed followed by compliance minimization with a volume constraint. For each optimization case we study both load cases individually, as well as the combined load case.

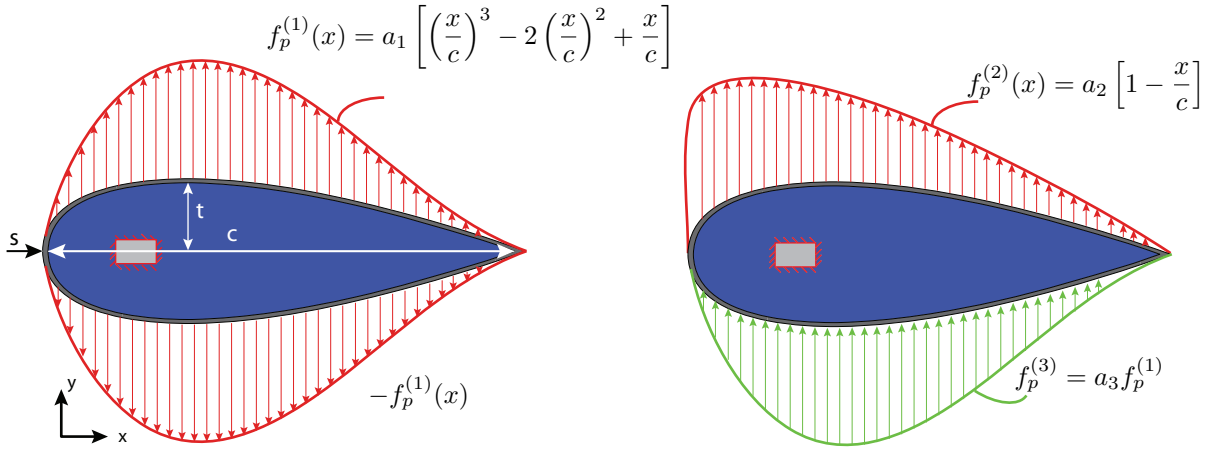

(a) Load case $\alpha = 0$.

(b) Load case $\alpha = 10$.

Figure 6: Load cases for two different angles of attack

The simplified loading conditions correspond to different angles of attack ($\alpha = 0$ and $\alpha = 10$) and are used here for illustrative purpose only. Parameters defining the geometry and loadings applied to the structure are listed in Table 2.

Table 2: Geometry and Loads.

	Loads	
Geometry	Coefficient	Resultant force
chord width $c = 1$	$a_1 = 15/12$	$F_1 = 1/15$
max. thickness $t = 0.3$	$a_2 = 1/15$	$F_2 = 1/30$
skin thickness $s = 1/60$	$a_3 = 1/4$	$F_3 = 1/60$

As in the L-bracket example, the design is discretized using quadrilaterals with bilinear shape functions. We assume plane stress linear elasticity. The airfoil is modeled by 120 elements along the chord length and 36 elements along the maximum thickness. We use a Young's modulus of $E = 1e4$ and a Poisson's ratio of $\nu = 0.3$. Furthermore, the skin is modeled by 'non-design' elements, which have the material properties of solid material elements ($\rho = 1$). These elements do not form part of the design domain. However, their stress values also have to satisfy the stress constraints and, consequently, do contribute to the global stress function. For the stress constraint implementation the same parameters are used as for the L-bracket: $P = 12$ and $\varepsilon_{qp} = 0.8$. Here, a maximum allowable stress is assumed of $\sigma_{\text{lim}} = 80$. The constrained optimization problem is solved using a gradient projection method based on a fixed density change in every iteration (0.1).[14] As a stopping criterion a fixed number (600) of topology optimization iterations is used. The initial data for both load cases are given in Table 3.

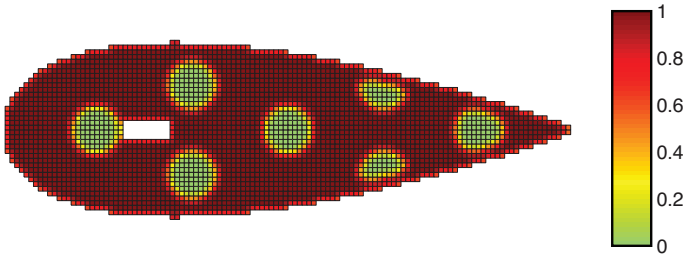

Figure 7: Initial density distribution.

Table 3: Initial data for initial design for each load condition.

Load Case	$\max \sigma_{\text{vm}}$	Compliance
$\alpha = 0$	17.51	0.30
$\alpha = 10$	92.72	1.71

First, volume minimization subjected a single global stress constraint is considered for each load case individually, $m = 1$ in Eq. (12). For the combined load case, an additional constraint is added to the problem and the design problem is defined as,

$$\begin{aligned} \min_{\boldsymbol{\phi}} V &= \frac{1}{n}\sum_{e=1}^{n}\rho_e \\ g_i &= \frac{c_i \sigma_{\text{PN}}(\mathbf{u}_i)}{\sigma_{\text{lim}}} - 1 \leq 0, \quad \text{for} \quad i = 1..2, \\ & \rho_{\min} \leq \rho_j \leq 1, \qquad \text{for} \quad j = 1..n, \end{aligned} \tag{13}$$

where $\mathbf{u}_i$, $\sigma_{\text{PN}}(\mathbf{u}_i)$ and g_i are the displacement vector, the aggregated stress function and the group constraint belonging to the i-th load case, respectively. Finally, the airfoil is optimized again by minimizing compliance subjected to a volume constraint to illustrate the differences between strength-based and stiffness-based design. Again, the load cases are studied individually, as well as combined. In this case, the volume values obtained in the stress-based case are used as volume constraints.

For compliance minimization of a design under multiple load cases, generally two types of formulations are used:[24] minimization of the maximum compliance with respect to the loading condition or minimize a (weighted) sum of the compliances of both load cases. Here, the latter is used and the design problem is defined as,

$$\begin{aligned} \min_{\boldsymbol{\phi}} C &= \sum_{i=1}^{2} \mathbf{u}_i^{\text{T}} \mathbf{K} \mathbf{u}_i \\ g &= \frac{V}{V_{\text{lim}}} - 1 \leq 0, \\ & \rho_{\min} \leq \rho_i \leq 1, \qquad \text{for} \quad i = 1..n, \end{aligned} \tag{14}$$

where C is defined as the sum of the compliances for each individual load case.

A. Stress-based design

The optimized designs for a single loading conditions are shown in Figure 8. For each loading condition a different design was obtained. The design for the first load case ($\alpha = 0$) converged to a relative volume of $V = 12.03\%$ and is made out of vertical members which are fully stressed as can be seen in Figure 8(a). The maximum stress is $\tilde{\sigma}^{\max} = 80.13$ and the constraint is thus slightly violated. For the second load

case ($\alpha = 10$) the optimized design converged to $V = 28.24\%$ has completely different design, which is a combination of diagonal and vertical members. Furthermore, note there still exists a relatively large region of low stress material connected to the leading edge, which appears to be suboptimal.

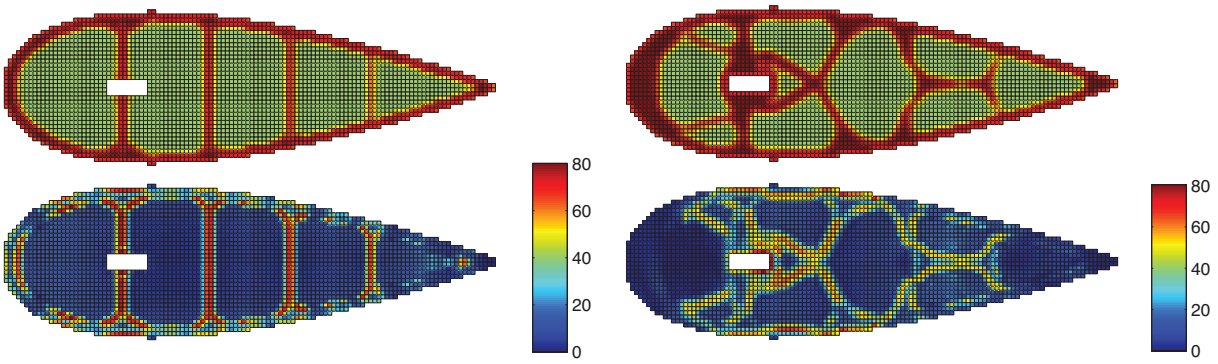

(a) Stress-based design for load case $\alpha = 0$ in Figure 6(a).

(b) Stress-based design for load case $\alpha = 10$ in Figure 6(b).

Figure 8: Stress-based design for the two loading conditions individually. On top the material distribution is shown and on bottom the corresponding Von Mises stress belonging to the applied load case.

The optimized design for the combined load case is shown in Figure 9. It can be seen that the design shows more resemblance with the second load case $\alpha = 10$. Both structures have the same topology. However, the diagonal members in the mid area between the spar connection and the trailing edge did change in shape and are in between the designs for the two individual load cases. The data for the each single load case and the combined case are listed in Table 4.

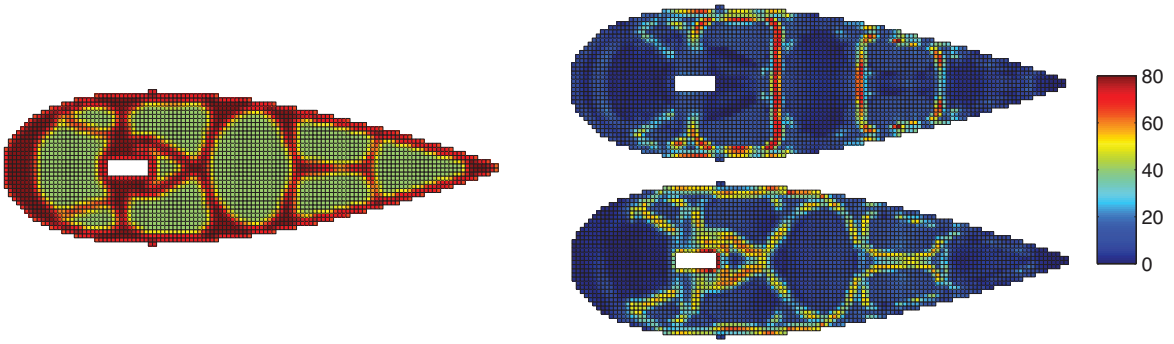

(a) Density distribution.

(b) On top and bottom, the Von Mises stress field for load case 1 and load case 2 are shown, respectively.

Figure 9: Stress-based design for the two loading conditions combined.

When minimizing volume, the stress constraint for the second load case $\alpha = 10$ is more critical. The stress constraint of the first load case becomes first active and therefore the optimizer only follows this constraint surface until the moment that the second constraint becomes active. Therefore, the design for the combined load case shows more resemblance with the second load case $\alpha = 10$. The design is also less optimal in terms of weight than the other two designs which is most likely a results of the fact that the shape of the members is now less optimal for the second load case $\alpha = 10$ (which becomes critical first). To compensate for this less mass was removed from the structure.

Table 4: Stress-based design for different load cases.

Load Case	Volume (%)	max σ_{vm}	Compliance
$\alpha = 0$	12.03	80.13	6.99
$\alpha = 10$	28.24	80.44	6.74
Combined*	30.04	80.15/80.53	4.67/6.30

* For the combined case, the two entries for stress and compliance correspond to load case $\alpha = 0$ and $\alpha = 10$, respectively.

B. Compliance-based design

Next, we perform a compliance-based optimization of the airfoil. The optimized volumes obtained in the previous section (listed in Table 4) are used here as volume constraints. These are: $V^1_{\text{min}} = 12\%, V^2_{\text{min}} = 28\%$ and $V^3_{\text{min}} = 30\%$, for the load case $\alpha = 0$, load case $\alpha = 10$ and the combination of these two, respectively. For the combined load case the objective function was taken as the sum of the compliances for both individual load cases. The optimized designs for the single load cases are shown in Figure 10.

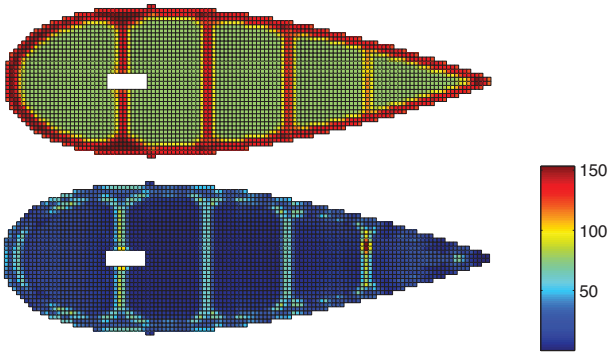

(a) Optimized design for load case $\alpha = 0$ in Figure 6(a).

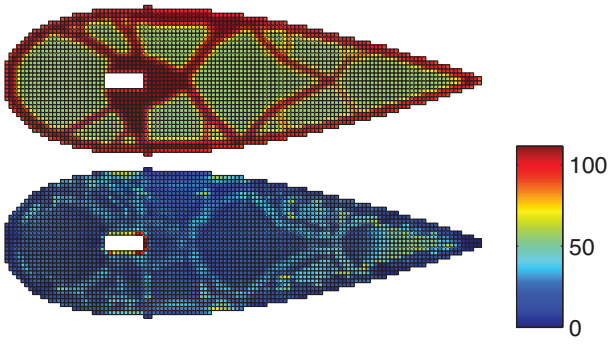

(b) Optimized design for load case $\alpha = 10$ in Figure 6(b).

Figure 10: Compliance-based design for the two loading conditions individually. On the top row the density distributions are shown for the final design. On the bottom row the corresponding stress state.

It can be seen that the optimized design for the first load case $\alpha = 0$ in Figure 10(a) is almost identical to the stress-based design in Figure 8(a). However, there is a local peak stress since no stress constraints are taken into account. The design for the second load case $\alpha = 10$ in Figure 10(b) is mainly made out of diagonals and shows resemblance with the stress-based design in Figure 8(a). However, its topology differs from the stress-based design. Furthermore, the design is more asymmetric which corresponds with the fact that the load is asymmetric. Also from comparing the stress distributions it can be seen that this is less uniform than in the stress based design.

For the combined load case the optimized compliance-based design is shown in Figure 11. This structure looks like a combination of the optimized designs of the individual load cases. In contrary to stress-based design for a multiple load case which showed much more resemblance with the second load case ($\alpha = 10$) since this became critical earlier in the design optimization process. This can be explained by the fact that, for the combined load case, the objective function used in Eq. (14) is defined as the sum of the compliances. In Table 5 the data are listed for each load case. It can be seen that the compliances for the combined load case are of the same order and therefore are both reflected in the final design.

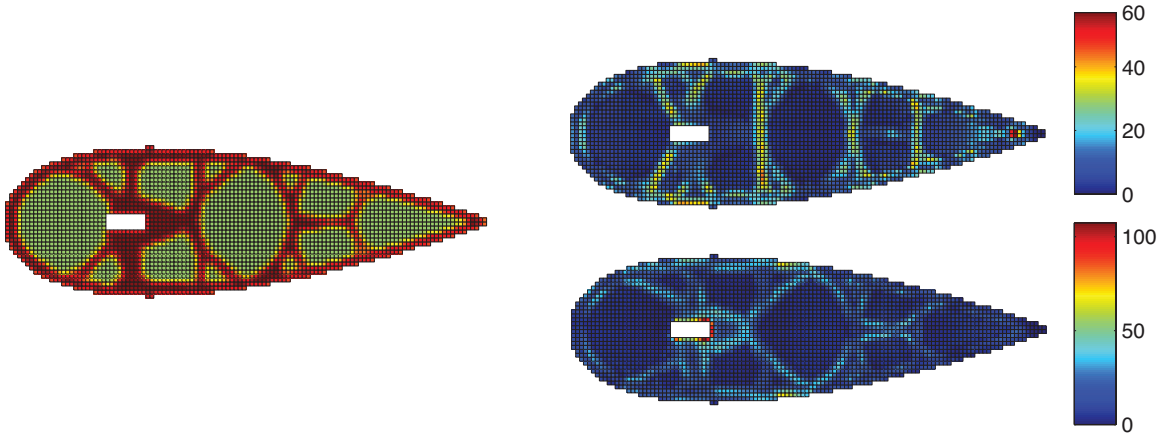

(a) Density distribution.

(b) On top and bottom, the Von Mises stress field for the first load case ($\alpha = 0$) and second load case ($\alpha = 10$) are shown, respectively.

Figure 11: Compliance-based design for the two loading conditions combined.

Furthermore, it can be seen from Table 5, that for each load case the maximum allowable stress limit is exceeded. It can be observed that the optimized design for the combined load case is non-optimal in terms of distributing the stress since there is a large difference between the maximum stress values for each load case, $\tilde{\sigma}^{\max}(\mathbf{u}_1) = 57.08$ vs. $\tilde{\sigma}^{\max}(\mathbf{u}_2) = 107.35$.

Table 5: Compliance-based design for different load cases.

Load Case	Volume (%)	$\max \sigma_{\text{vm}}$	Compliance
$\alpha = 0$	12.00	153.43	7.09
$\alpha = 10$	28.00	111.68	3.64
Combined*	30.29	57.08/107.35	2.10/4.12

* For the combined case, the two entries for stress and compliance correspond to load case $\alpha = 0$ and $\alpha = 10$, respectively.

C. Dependence on initial design

One of the major difficulties we have observed is the strong dependence on its initial design. Especially, for stress constraints we observed this problem. This will be illustrated by repeating stress-based optimization for the second load case ($\alpha = 10$) for a different initial design shown in Figure 12. Instead of the coarse distribution of large holes in Figure 7, we use a refined initial design with a increased number of smaller holes.

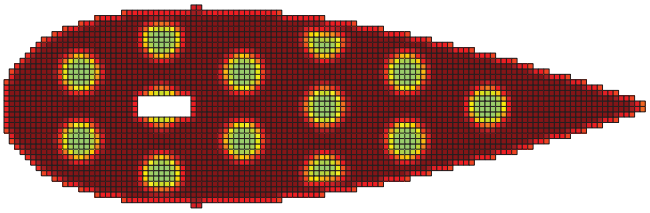

Figure 12: Refined initial design with an increased number of smaller holes.

In Figure 13, the optimized designs for both initial conditions are shown with the corresponding Von Mises stress distribution. On the top row the optimized design for the original coarse mesh and on the bottom row for the refined mesh. The results are listed in Table 6.

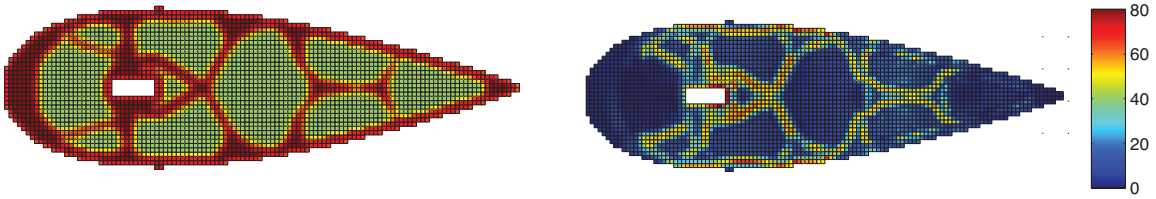

(a) Optimized design for initial design in Figure 7.

(b) Von Mises stress.

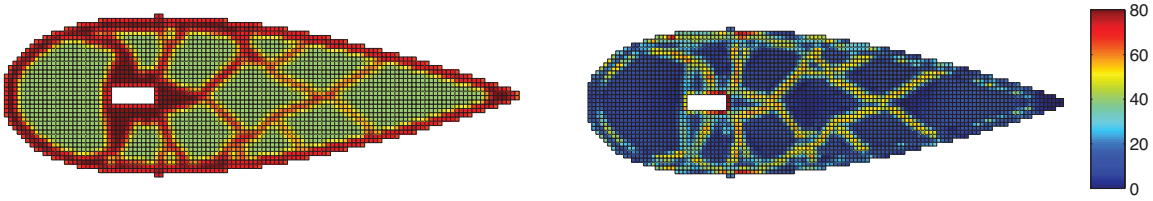

(c) Optimized design for initial design in Figure 12.

(d) Von Mises stress.

Figure 13: Stress-based design for load case $\alpha = 10$, obtained for two different initial designs. On the top row the optimized design is shown for the coarse distribution of holes and on the bottom row the optimized design is shown for the refined initial design.

It can be seen that the their is a large difference between the two optimized structures in Figure 13. For the refined initial design the optimized design contains more thin members and is more optimal in terms of the volume objective. Both designs lead to a more or less uniform stress distribution for the applied load case as can be seen from Figure 13(b) and Figure 13(d).

Table 6: Stress-based design for different load cases

Load Case	Volume (%)	$\max \sigma_{\text{vm}}$	Compliance
$\alpha = 10$	28.24	80.44	6.74
$\alpha = 10$	24.17	80.15	6.26

VI. Conclusions and future work

Our preliminary results show that level set based optimization with a consistent sensitivity analysis can be used effectively for stress-constrained problems with (multiple) constraints. For both numerical benchmark problems we obtained stress-based designs that meet the maximum allowable stress criterion very closely. Furthermore, for the airfoil design subjected to multiple loading, we obtained a stress-based design which is effective for both loading conditions, i.e. the maximum stress for both loading conditions is close to the maximum allowable stress. It was also shown that this design may be very different from the minimum compliance-based design, especially for the multiple load case.

Furthermore, it was shown by comparing convergence histories, that inconsistencies introduced by scaling of the P-norm in combination with 'swapping' of elements between group constraints, have a negative effect on convergence. This appears to become more critical when increasing the number of group constraints. Therefore, a careful choice should be made for an adaptive scaling update scheme.

One of the major difficulties when considering stress constraints is that due to their non-linear nature these problems are prone to convergence to inferior local minima and highly depend on the initial design. In

this level set description in which all changes occur along the boundary we also observed a strong dependence on the initial design.

For future research, we will compare the results obtained with this method to results obtained by SIMP. Furthermore, we will investigate how to improve scaling and subdivision in group constraints and limit the effect of such inconsistencies.

References

[1]Bendsøe, M., "Optimal shape design as a material distribution problem," *Structural and multidisciplinary optimization*, Vol. 1, No. 4, 1989, pp. 193–202.

[2]Zhou, M. and Rozvany, G., "The COC algorithm, Part II: topological, geometrical and generalized shape optimization," *Computer Methods in Applied Mechanics and Engineering*, Vol. 89, No. 1, 1991, pp. 309–336.

[3]Bendsøe, M. and Sigmund, O., *Topology optimization: theory, methods, and applications*, Springer Verlag, 2003.

[4]Krog, L., Tucker, A., and Rollema, G., "Application of topology, sizing and shape optimization methods to optimal design of aircraft components," *Airbus UK Ltd, Altair Engineering Ltd*, 2002.

[5]Rozvany, G. and Birker, T., "On singular topologies in exact layout optimization," *Structural and Multidisciplinary Optimization*, Vol. 8, No. 4, 1994, pp. 228–235.

[6]Sved, G. and Ginos, Z., "Structural optimization under multiple loading," *International Journal of Mechanical Sciences*, Vol. 10, No. 10, 1968, pp. 803–805.

[7]Rozvany, G., "On design-dependent constraints and singular topologies," *Structural and Multidisciplinary Optimization*, Vol. 21, No. 2, april 2001, pp. 164–172.

[8]Duysinx, P. and Sigmund, O., "New Developments in Handling Stress Constraints in Optimal Material Distributions," *Proceedings of 7th AIAA/USAF/NASA/ISSMO symposium on Multidisciplinary Design Optimization*, AIAA, 1998.

[9]Yang, R. J. and Chen, C. J., "Stress-based topology optimization," *Structural and Multidisciplinary Optimization*, Vol. 12, No. 2, 1996, pp. 98–105.

[10]Duysinx, P. and Bendsøe, M., "Topology optimization of continuum structures with local stress constraints," *International Journal for Numerical Methods in Engineering*, Vol. 43, No. 8, 1998, pp. 1453–1478.

[11]Rozvany, G., "Difficulties in truss topology optimization with stress, local buckling and system stability constraints," *Structural and Multidisciplinary Optimization*, Vol. 11, No. 3, 1996, pp. 213–217.

[12]Cheng, G. and Guo, X., "ε-relaxed approach in structural topology optimization," *Structural and Multidisciplinary Optimization*, Vol. 13, No. 4, 1997, pp. 258–266.

[13]Bruggi, M., "On an alternative approach to stress constraints relaxation in topology optimization," *Structural and Multidisciplinary Optimization*, Vol. 36, No. 2, 2008, pp. 125–141.

[14]van Dijk, N., Langelaar, M., and van Keulen, F., "Level-set-based topology optimization using an exact Heaviside function and consistent sensitivity analysis," *Proceedings of the 9th World Congress of Structural and Multidisciplinary Optimization WCSMO9*, 2011.

[15]van Dijk, N., Langelaar, M., and van Keulen, F., "Explicit level-set-based topology optimization using an exact Heaviside function and consistent sensitivity analysis," In press.

[16]Amstutz, S. and Novotny, A., "Topological optimization of structures subject to Von Mises stress constraints," *Structural and Multidisciplinary Optimization*, Vol. 41, No. 3, 2010, pp. 407–420.

[17]Guo, X., Zhang, W., and Wang, M., "Stress-related Topology Optimization via Level Set Approach," *Proceedings of the 9th World Congress of Structural and Multidisciplinary Optimization WCSMO9*, 2011.

[18]Wang, M., Wang, X., and Guo, D., "A level set method for structural topology optimization," *Computer methods in applied mechanics and engineering*, Vol. 192, No. 1, 2003, pp. 227–246.

[19]Liu, Z., Korvink, J., and Huang, R., "Structure topology optimization: fully coupled level set method via FEMLAB," *Structural and Multidisciplinary Optimization*, Vol. 29, No. 6, 2005, pp. 407–417.

[20]Allaire, G., Jouve, F., and Maillot, H., "Topology optimization for minimum stress design with the homogenization method," *Structural and Multidisciplinary Optimization*, Vol. 28, No. 2-3, 2004, pp. 87–98.

[21]Le, C., Norato, J., Bruns, T., Ha, C., and Tortorelli, D., "Stress-based topology optimization for continua," *Structural and Multidisciplinary Optimization*, Vol. 41, No. 4, 2010, pp. 605–620.

[22]París, J., Navarrina, F., Colominas, I., and Casteleiro, M., "Block aggregation of stress constraints in topology optimization of structures," *Adv. Eng. Softw.*, Vol. 41, No. 3, 2010, pp. 433–441.

[23]Verbart, A., van Dijk, N., Del Tin, L., Langelaar, M., and van Keulen, F., "Effect of design parameterization and relaxation on model responses in topology optimization with stress constraints," *Proceedings of the 9th World Congress on Structural and Multidisciplinary Optimization*, 2011.

[24]Rozvany, G., "Stress ratio and compliance based methods in topology optimization a critical review," *Structural and Multidisciplinary Optimization*, Vol. 21, 2001, pp. 109–119.